# Early-time regime for interfacial instabilities in a kinetic Ising model

Loki Jörgenson, H. Guo, R. Harris, and M. Grant
*Department of Physics and Center for the Physics of Materials, McGill University, Rutherford Building, 3600 University Street, Montréal, Québec, Canada H3A 2T8*
(Received 26 April 1993)

We have applied a Monte Carlo method to study the interfacial dynamics of a two-phase Ising lattice-gas system in two dimensions. Planar and circular interfaces are driven into nonequilibrium by a temperature gradient, and unstable modes develop causing one phase to grow into the other. We study the instability of the interface by monitoring the growth of these modes. In the case of a planar interface, a long-range interaction between the sites results in an extended linear regime where the modes grow exponentially in time, whereas, in the circular case, they grow only after the solid disk has exceeded a critical radius. We compare the data with linear stability analysis and find good agreement.

PACS number(s): 68.10.−m, 82.65.Dp

## I. INTRODUCTION

The formation and evolution of dynamic structures is one of the most exciting areas of nonlinear phenomenology. Pattern-formation problems are common in various fields, including hydrodynamics, biology, metallurgy, and combustion. The best studied pattern-formation problems involve growing interfaces between two phases: a solid and a fluid, or two fluids. Specific systems that have received much attention over the last several years include viscous fingering in a Hele-Shaw cell [1–3], directional solidification of binary systems [4, 5], and dendritic growth of a solid from a melt [6]. All of these systems have the feature that between two phases there exists a moving boundary upon which act competing stabilizing and destabilizing forces. The physical origins of these forces depend on the particular system under investigation. For instance, in the case of dendritic crystal growth, thermal gradients destabilize the interface separating the solid and the liquid while surface tension tries to stabilize it. It is the interplay between the two which leads to the pattern observed.

A particular interfacial instability, first studied by Mullins and Sekerka [7, 8], lies at the heart of a variety of pattern-formation processes. In the case of a solid growing into a supercooled melt, the instability is driven by the diffusion of heat through the interface. Mathematically, the interface evolves through a nonlinear coupling to a diffusion field, and accordingly, a planar interface is linearly unstable to long-wavelength perturbations, but linearly stable against short-wavelength perturbations.

Considerable progress has been made in the past few years regarding the difficult problem of steady-state pattern selection in certain systems [9, 10]. However, relatively little attention has been paid to the early- or intermediate-time regime [11–14] where the dynamics of the interfacial instability plays a vital role. Due to their inherent nonlinearity and nonlocality, interfacial instability problems, in general, resist even numerical attack. Thus a promising alternative approach is through lattice-based computer simulations [12, 15]. Once an appropriate lattice model is constructed, it can, in principle, be used to study the complete dynamics of the pattern-forming process, from an initially planar interface to a final steady state. A successful example is the lattice-gas automaton developed by Kadanoff [16] to study the viscous-fingering problem [17–19].

In a series of papers [15–24], we have successfully developed a Monte Carlo method to study interfacial dynamics driven by a temperature gradient. Our model is a two-phase Ising lattice gas which has been modified to give an interface between coexistent phases. It also has been coupled to a temperature field, thus providing a driving force via a thermal gradient. It is found that dendritic shapes form and eventually develop into a steady state. The characteristic wavelength of the steady-state pattern is established very early in the instability during the linear early-time growth; we have measured it at late times and found it consistent with analytic theory [25]. Lattice-gas simulations like ours have additional advantages such as simple boundary conditions and an inherent crystal anisotropy [24].

In this paper, we present results of a further simulation in two dimensions which focus primarily on the early-time regime where linear stability analysis of the continuum equations is expected to be valid. While linear stability analysis is a powerful and much utilized method for the study of interfacial dynamics, very little has been done to simulate the linear regime directly. This is because an interface driven unstable usually passes through to the nonlinear regime very quickly before the linear regime is detectable. In this paper we show that our simulation of dendritic crystal growth can quantitatively be compared with linear stability analysis. This is a further indication that the model captures the essential physics of the instability, and can provide invaluable insights into its nature.

We have examined two different two-dimensional geometries: a circular geometry where the initial crystal seed is a disk, and a planar geometry where the initial

 

interface is flat. In the case of the planar geometry, the linear regime is not observed unless we increase the range of the interaction within our Hamiltonian. This occurs because the instability is suppressed by the longer-range force and consequently the duration of the linear regime is extended. In the case of circular geometry, the surface of the circular crystal cannot support any instability until its radius $R$ grows to be larger than a critical radius $R^*$. Consequently the duration of the linear regime can be controlled directly through the driving force, and the long-range interaction is not necessary. The development of $R$ as a function of time is followed until the interface becomes unstable and is compared with the predictions of linear stability analysis.

The outline of the rest of the paper is as follows. Section II presents the model and the method of simulation. Section III summarizes the results and gives the comparison between our data and the predictions of a linear stability analysis. Section IV is reserved for a short discussion and summary.

## II. THE MODEL AND THE ALGORITHM

The continuum description of dendritic crystal growth is well known in the literature [9, 10] and here is only briefly summarized. The solid-liquid interface is considered to be a discontinuous surface for the temperature field. This is justified since the interface is in general very thin. As the solidification progresses, latent heat is released, diffuses away from the interface, and drives the interface unstable. Although this process is far from equilibrium, the interface itself can often be considered to be in local equilibrium, since the time scale of condensation and evaporation at the interface is much shorter than the time scale for heat diffusion. This is referred to as the quasistatic approximation.

The interface behavior is fully described by Eqs. (1)–(3) where the temperature field is represented by the dimensionless quantity $u \equiv c(T - T_m)/\lambda$, where $c$ is the specific heat, $T_m$ is the coexistence temperature and, $\lambda$ is the latent heat of transition per unit volume:

$$\frac{\partial u}{\partial t} = D\nabla^2 u \ , \tag{1}$$

$$u_\perp = -d_0\kappa \ , \tag{2}$$

$$\lambda v_n = Dc[(\nabla u)_{\rm sol} - (\nabla u)_{\rm liq}] \cdot \mathbf{n}. \tag{3}$$

$D$ is the thermal diffusion constant of both the liquid and solid phases. Equation (2) is the Gibbs-Thomson relation which provides the thermodynamic boundary condition at the interface in terms of the capillary length $d_0 \equiv \gamma T_m c/\lambda^2$ with $\gamma$ the surface tension and $\kappa$ the local interface curvature. Equation (3) is the heat conservation relation (the heat generated by solidification must flow into the bulk material) with $v_n$ the normal interface velocity and $\mathbf{n}$ the unit vector normal to the interface. Equations (1)–(3) are nonlinear since the boundary condition (2) depends on time through $\kappa$. In principle, there are corrections to the local equilibrium assumption, Eq. (2), due to kinetic effects, such that velocity-dependent terms appear, but for simple analysis, these effects are generally neglected.

On a planar interface, a linear stability analysis of Eqs. (1)–(3) can be carried out by assuming that the interface is represented as a single-valued function $h$ of the transverse coordinate $\mathbf{x}$ and time $t$:

$$h(\mathbf{x}, t) \sim \sum_k e^{i\mathbf{k}\cdot\mathbf{x}+\omega_k t}. \tag{4}$$

Following Langer [25], if the normal velocity of the unperturbed interface is $v_n$, then the thermal diffusion length can be defined as $l \equiv 2D/v_n$. In the quasistatic limit $kl >> 1$ and when $kd_0 \ll 1$, the dispersion relation between the frequency $\omega_k$ and wave number $k$ is then found to be

$$\omega_k \approx kv_n[1 - d_0 l k^2] \ . \tag{5}$$

Two regimes are defined by the critical wavelength

$$\lambda_c = 2\pi\sqrt{d_0 l}. \tag{6}$$

Modes with wavelength $\lambda > \lambda_c$ will be damped out, but modes with $\lambda < \lambda_c$ will grow exponentially in time, the wavelength $\lambda_{\rm max} = \sqrt{3}\lambda_c$ growing fastest, giving rise to the Mullins-Sekerka instability.

Note that the critical length scale $\lambda_c$ is the geometric mean of two vastly different length scales. For a real experimental system, $d_0$ is of order angstroms while $l$ can be as large as millimeters. This poses a fundamental difficulty for any simulation based on microscopic models, since it is hard, if not impossible, to model the two length scales with several orders of magnitude difference in value. Consequently, there is some doubt whether the linear regime of the Mullins-Sekerka instability can reasonably be simulated in the quasistatic limit. This point is further discussed below.

With a planar interface, there is an additional problem posed by the brevity of the linear regime. That this is so follows from the expression for the perturbed thermal field, which must have the form

$$u(t) \propto e^{\omega_k t} + O(h), \tag{7}$$

where $O(h)$ is a correction caused by the perturbation of the interface. Since, from (4), this correction must also have the form $h(\mathbf{x}, t) \sim e^{\omega_k t}$, the perturbation expansion of Eq. (7) is singular, suggesting that the linear behavior will indeed be difficult to observe.

To estimate the duration of the linear regime, we assume, following Binder [26, 27], that the model system incorporates interactions with a range $\varrho$. In the linear regime, we therefore expect correlations of size $\varrho$, and a critical wave number of size $1/\varrho$. A mode with this wave number, from Eq. (5), will grow like $e^{v_n t/\varrho}$, so that the correction term in (7) will be unimportant only when $e^{v_n t/\varrho} \ll \varrho$, or when

$$t \ll \tau_{\rm lin} \sim \frac{\varrho}{v_n} \ \ln(\varrho).$$

The time $\tau_{\rm lin}$ measures the duration of the linear regime: Increasing the range of the interaction $\varrho$ will clearly increase its value.

For circular geometry, the linear stability analysis is

carried out by studying the growth of a disturbance on a perfect circle of radius $R_0$,

$$R(\theta) = R_0 + \sum_m \delta_m \cos(m\theta) e^{\omega_m t}.$$

We present a complete analysis in the Appendix. In the linear regime the modes $m$ decouple and become unstable, with $\omega_m > 0$ when the disk radius $R_0$ is larger than the critical radius

$$R_m^* = \sqrt{m(m+1)d_0 l} \tag{8}$$

$$= R_c[1 + 2m(m+1)]. \tag{9}$$

Here $R_c$ is the critical radius for nucleation, such that the droplet shrinks for $R < R_c$ but grows for $R > R_c$. Thus, assuming that the first instability sets in at the lowest growth mode with $m = 2$, the disk becomes unstable at $R_2^* = \sqrt{6d_0 l}$. In this case, the simplest test of linear behavior is to calculate $R_m^*$ for a given system and compare it to the simulation results.

## III. THE SIMULATIONS

### A. The model

Our microscopic model is a lattice gas on a square lattice described by a Hamiltonian

$$H = -J \sum_{<ij>} S_i S_j - \Delta \sum_i S_i, \tag{10}$$

where $J$ is the interaction strength; the spin variables $\{S_i\} = \{\pm 1\}$ describe the solid $(+1)$ or liquid $(-1)$; $\Delta$ is an external field. The spin-spin interaction for each site $S_i$ is calculated within a diamond-shaped area centered at site $i$. The number of spins interacting with $S_i$ is $2\rho(\rho+1)$ where $2\rho$ is the length of the diamond's axes. Thus, $\rho$ represents the effective range of interaction (e.g., $\rho = 1$ for nearest-neighbor interactions). To introduce a first-order transition we assign each *down* $(-1)$ spin state a $\delta$-fold degeneracy [15, 28]. It is then easy to show that a first-order transition occurs at a temperature $T_M = 2\Delta/\ln\delta$ provided that $T_M$ is less than the second-order transition temperature of the Ising model with long-range interactions. A latent heat with value approximately equal to $2\Delta$ is produced at the first-order transition.

Since heat diffusion is essential for the instability, a conventional Metropolis Monte Carlo [29] method with temperature $T$ fixed is inadequate for our purpose. Thus a variant of the microcanonical Monte Carlo method [30] is used with, the spin system in contact with an auxiliary system of noninteracting *demons*. There is a one-to-one correspondence between the spins and the demons. Each demon has a non-negative energy $\epsilon_d$ and energy is exchanged between the spins and demons such that the total energy is conserved. Spins are visited one at a time at random, and at each site, a spin flip to the other phase is attempted; a Monte Carlo step (MCS) is complete when every site has been visited once. The potential change in energy $\triangle\epsilon_d$ for each flip is calculated and compared with the energy available from the demon which corresponds to the current site. The value of $\triangle\epsilon_d$ determines the course of action, as follows:

$$\begin{array}{ll} \triangle\epsilon_d < 0, & \text{flip and demon absorbs energy} \\ 0 < \triangle\epsilon_d < \epsilon_d, & \text{flip and demon gives up energy} \\ \epsilon_d < \triangle\epsilon_d, & \text{no flip and no change in demon energy.} \end{array} \tag{11}$$

This algorithm results in the redistribution of demon energy and consequently represents a thermal diffusion process. Since a nonconserved order parameter $(\sum_i S_i)$ is coupled with a conserved field (energy), the dynamics corresponds to model $C$ in critical dynamics [31].

The boundary conditions are similar to those described in our other publications [20, 22, 23]. The solid and liquid phases are initialized at the coexistence temperature $T_m$ and at some undercooled temperature $T < T_m$, respectively. Periodic boundary conditions apply on all four sides except that the planar simulations fix two opposite edges of the system to belong to opposite phases. The edges are maintained at the appropriate temperatures, as if in contact with heat baths, using a Metropolis method.

### B. The planar case

Our data was from a planar interface of size $8196 \times 28$ at $T_m = 2.0J$ with an undercooling in the liquid melt of $T = 0.45J$. The spin degeneracy was $\delta = 3$ with a latent heat of transition $\lambda = 1.22J$. A range of interaction of $\rho = 3$ was used resulting in a linear regime of an approximate duration of 1000 MCS. The interface was initially brought to equilibrium at $T = T_m$ and then allowed to evolve for 1000 Monte Carlo steps in the presence of a thermal gradient. As the interface instability developed, the Fourier spectrum of modes was measured. Figure 1 shows a time series of a typical one dimensional (1D) planar interface during the linear stages of the instability. In an earlier study [15], we examined the late-time behavior of a similar interface using the same model and comparable system parameters; we observed dendritelike fingers with a characteristic length scale, consistent with the conventional picture of the Mullins-Sekerka instability.

As in previous studies [15, 21], the most informative method for analyzing the interface is via the power spectrum of its fluctuations, defined as

$$P(k) \equiv |\mathcal{F}\{h(x)\}|^2 , \tag{11}$$

where $\mathcal{F}\{h(x)\}$ is the spatial Fourier transform of the interface position in one dimension. Figure 2 shows a time series of the power spectra, averaged over 400 trials, for $t = 100, 500$, and 1000 MCS. Note the modes at high $k$ which are typical of interface roughening. The solid line

FIG. 1. A time series of the 2D planar instability with long-range interactions. The system size is $8196 \times 24$ but only a section $550 \times 24$ is shown here.

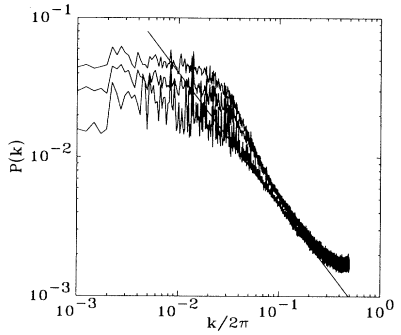


FIG. 2. The power spectra of the unstable planar interface at $t = 100$, 500, and 1000 MCS as shown in Fig. 1. The wave number $k$ is in units of the inverse lattice spacing. Note the static modes at high $k$ which are characteristic of interface roughening. The solid line approximates the steady-state roughening modes.

represents the steady-state roughening level, and thus the modes which extend above it are the growth modes; the area between the solid line and the curve(s) is the excess power attributed to the instability.

We are looking for an exponential time dependence of the modes. As we can see from Fig. 3, the behavior of typical modes is more or less consistent with our expectations. The growth of the higher-$k$ modes is weaker and less defined, saturating at late time. Also, the occasional $k$ mode like that shown in Fig. 3(c) appears to have been initialized with too high an amplitude; it exhibits an early-time transient as it quickly relaxes to local equilibrium and begins to grow normally.

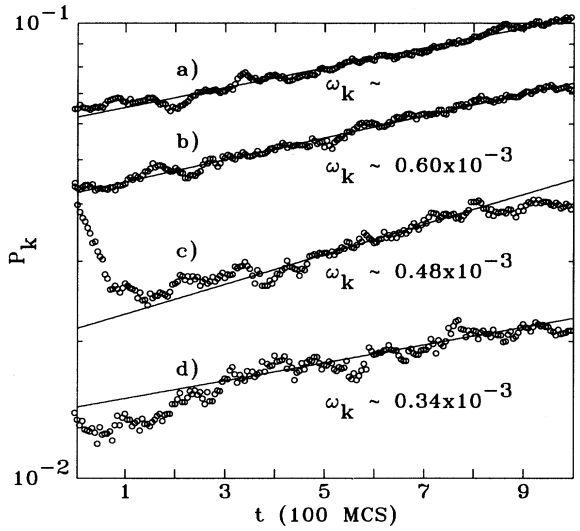


FIG. 3. Semilogarithmic plots of some typical growth modes below the critical mode $k_c/2\pi \sim 0.060$; (a) $k/2\pi \sim 0.014$, (b) $k/2\pi \sim 0.024$, (c) $k/2\pi \sim 0.038$, and (d) $k/2\pi = 0.048$. The corresponding wavelengths for (a)–(d) are $74a, 41a, 26a$ and $21a$, respectively, where $a$ is the unit lattice spacing. The straight solid lines are fits to the form $e^{w_k t}$ as described in the text.

To extract the dispersion relation $\omega_k$, we fitted each mode individually, via a least squares algorithm, with an expression $Ae^{\omega_k t}$ where $A$ and $\omega_k$ were the fitting paramters. The very earliest and latest times were ignored to avoid the influences of poor initialization and saturation, respectively. In Fig. 4, we show $\omega_k$ for all of the $k$ modes in the power spectrum up to $k/2\pi \simeq 0.06$; errors in the fitted values are much smaller than the variations in these values because, despite the large number of runs (400), the noise is still significant. Modes with $k/2\pi > 0.06$ are not shown because they display no interesting behavior.

The measured dispersion relation differs in several respects from the theoretical expression (5) which is shown as the solid line in the inset to Fig. 4. First, decay modes beyond the critical wave vector $k_c$ are not represented; this is because they are overwhelmed by the equilibrium capillary modes, already present because of the initial conditions. Thus, we simply observe $\omega_k$ going to zero at $k_c$. Second, the measured $\omega_k$ shows no clear sign of a maximum: Indeed it shows no sign of the expected linear behavior as $k$ tends to zero. Taking $k_c/2\pi \sim 0.06$, and attempting to fit the data to Eq. (5), is equally disappointing: the characteristic asymmetric form of the dispersion relation is not consistent with data, even for $0.03 < k/2\pi < k_c/2\pi$.

Part of the difficulty is that the interesting region of the spectrum corresponds to wavelengths close to the system size: This is true even though the size, at $8196a$, is much larger than that used in our previous 2D work [22]. This causes the instability to occur not far from that

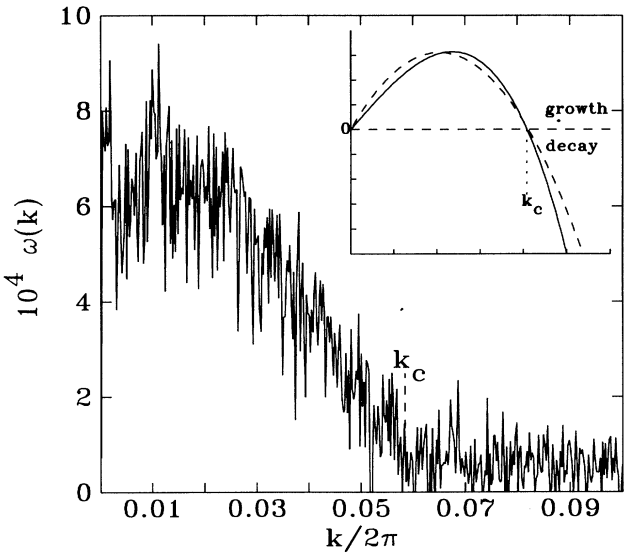


FIG. 4. The linear stability dispersion function from fits of the planar interface modes to the expected exponential behavior. The wave number $k$ is in units of the inverse lattice spacing. These results are based on 400 simulation trials of an $8196 \times 24$ system which employs a long-range interaction ($\rho = 3$). Error bars are much smaller than the noise. The inset shows the theoretical dispersion relations predicted by linear analysis (see text).

region of the spectrum where the capillary fluctuations take longest to come to thermal equilibrium [22,32]. It is clear from Fig. 2 that, even after the longest run times, the modes of the longest wavelength (say $k/2\pi < 0.01$) have not achieved amplitudes close to their equilibrium values.

However, a more fundamental difficulty is that, despite the large system size, the ratio between the diffusion length $l$ and the capillary length $d_0$ is not sufficiently large. Because of this, the power spectra show a close resemblance to those obtained at early times ($t < d_0^2/D$) for the roughening of a planar interface in the absence of a temperature gradient [22]. These spectra were interpreted in terms of a crossover between the early-time linear regime where the damping of modes is dominated by the surface tension, and the late-time linear regime where the damping is dominated by the diffusion of heat. Equation (5) corresponds to this latter regime, with a damping coefficient $\omega_k$ proportional to $-k^3$ for $kd_0 \ll 1$: it is therefore valid when $kd_0 \ll 1 \ll kl$ or $\alpha \ll 1$, with $\alpha = d_0/l$.

Thus, presumably, our data correspond to the regime where the condition $kd_0 \ll 1$ is not well satisfied, and the late-time regime $t > d_0^2/D$ has not been reached. It therefore seems appropriate to analyze the instability by linearizing the equations of motion (1)–(3) but treating $\alpha$ as a small parameter. After some algebra, following Langer and Appendix B of Ref. [22], the linearized equations to order $\alpha^2$ become:

$$\omega = \frac{D}{d_0^2}[2\alpha\tilde{q} - (2\tilde{q} - 2\alpha)\tilde{k}^2 - 4\alpha^2] ,$$

$$\omega = \frac{D}{d_0^2}(-\tilde{k}^2 + \tilde{q}^2 - 2\alpha\tilde{q}) ,$$

where $\tilde{k}$ and $\tilde{q}$ are $kd_0$ and $qd_0$, respectively.

The limit $\alpha = 0$, corresponding to the static, equilibrium interface, gives the results of Ref. [22]. Lowest order in $\alpha$, in the limit $kd_0 \ll 1$, gives Langer's result. When $\alpha$ is somewhat larger, the equations must be solved numerically, and give a much more symmetric dispersion relation, illustrated as the dashed curve in the inset to Fig. 4 for $\alpha = 0.1$.

While the dashed curve is not intended as a fit to the data, since $\alpha$ is unlikely to have a value as large as 0.1, it illustrates clearly the qualitative consequence of inadequate separation of the large and small length scales $l$ and $d_0$, in the simulation. The instability displayed by our data is well defined, but probably does not correspond to the classic Mullins-Sekerka situation.

### C. The circular case

The size of our simulation system was $128 \times 128$ with an initial circular inclusion of $R_0 = 5$ lattice units. The coexistence temperature was set to $T_m = 1.72J$. The undercooled temperature was $T = 0.40J$ with the spin degeneracy set to $\delta = 3.21$. Since long-range interaction is not necessary to observe the onset of the instability, the range was $\rho = 1$. These particular parameters were chosen by trial and error to give a specific rate of growth without homogeneous nucleation while producing an instability at a droplet radius within the system size. The statistics were derived from data averaged over 500 trials of 2500 MCS each, and the instability was observed to occur, on average, at $t \sim 1200$ MCS.

Figure 5 shows a time series for the growth of a typical droplet; note that although fluctuations appear before the indicated instability sets in, they are eventually damped out. Visual inspection shows that the disk becomes unstable at around $R \sim 20a$ where $a$ is the unit lattice spacing. Figure 6 shows the reference radius $R(t) \equiv \sqrt{N(t)/\pi}$, where $N$ is the total number sites associated with the droplet. $R(t)$ grows like $t^{1/2}$ [consistent with (A2) for a large undercooling] up to $t \simeq 1250$ MCS when $R(t)$ becomes linear in $t$. This corresponds to $R \sim 21a$.

We compare this result with the expressions (8) and (9) by two different procedures. First, we employ Eq. (9), estimating the critical radius $R_c$ from the surface energy $\gamma(T)$ and the bulk free energy $\triangle E_b(T)$ as described in the Appendix. Since there is some ambiguity in identifying the local temperature at the interface, we choose an intermediate value of $1.13J$. The surface energy is thus $\gamma(1.13J) \simeq 1.6J$ and the bulk free energy difference between the solid at $T = 1.72J$ and the melt at $T = 0.41J$ is $\triangle E_b \sim 0.73J$. This gives a critical nucleation radius of $R_c \sim 2.3a$. Thus, for the lowest possible mode $m = 2$, we predict the stability radius to be

$$R_2^* \sim 25a$$

whereas with $m = 4$ (appropriate, perhaps, to the square anisotropy of the lattice), we find $R_4^* \sim 93a$. Clearly the lowest growth mode dominates the instability.

A more direct measurement of $R_m^*$ can be made by carrying out a secondary simulation. Since a droplet at $R < R^*$ is always circularly stable, we can observe the *evaporation* of the droplet from an initial radius $R_0$ at the coexistence temperature $T_m$. We can fit the results from the simulation with (A2), treating $R_c$ as an unknown

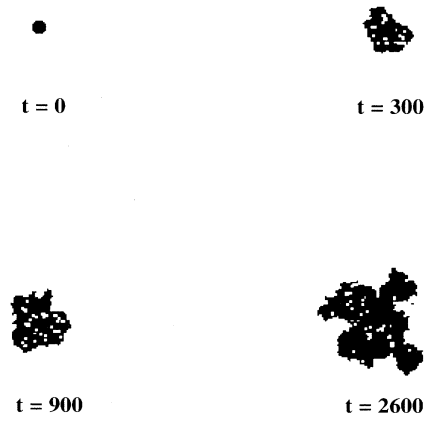


FIG. 5. A time series of the disk instability in 2D for a system of $256 \times 256$; images are for $t = 0, 300, 900$, and 2600 MCS. The disk remains circular up to the stability radius $R \sim 20a$ ($t \sim 1000$ MCS) where it becomes unstable.

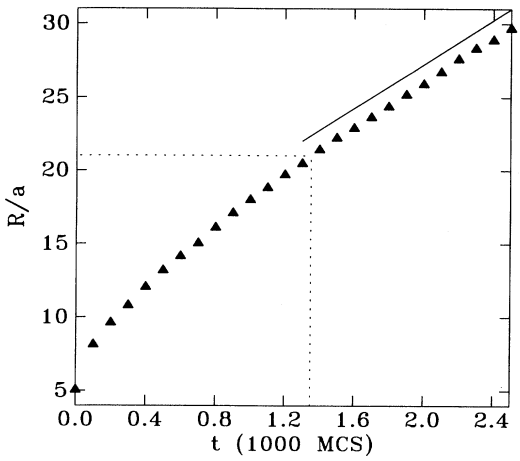


FIG. 6. The reference radius $R(t) \equiv \sqrt{N(t)/\pi}$ as a function of time for the disk instability. While the disk is circular, $R$ corresponds to the actual disk radius. When it becomes unstable and no longer compact, $R$ grows linearly in time.

constant, to find the product $d_0D$. Then we only need $v_R$ to establish $R_m^*$ from Eq. (8). Although $v_R$ is not strictly constant, it changes slowly and we can assign it a value for a given $R$.

Figure 7 shows the reference radius of an evaporating droplet from a typical simulation run for a $128 \times 128$ system with an initial droplet of size $R_0 = 50a$. The ambient temperature was set to the coexistence temperature $T_m = 1.72J$. From a fit of $R(t)$ using (A2), we find $(d_0D) \simeq 0.3$ ; note that we expect the poor fit at small $R$ (late time) due to finite size effects. From the first simulation data, we estimate the interface velocity in the neighborhood of the instability to be $v_R \simeq 0.009$ lattice units per MCS. This gives an instability radius

$$R_2^* \simeq 20a.$$

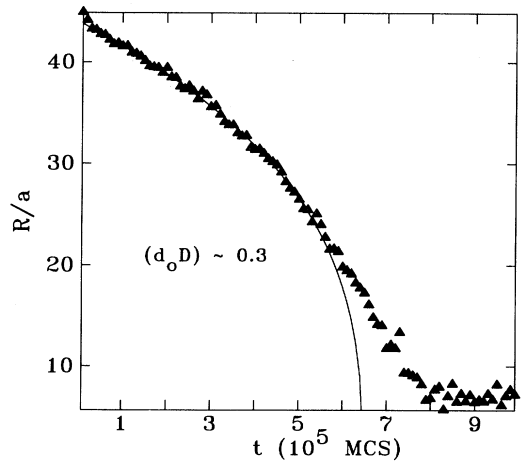


FIG. 7. The radius $R(t)$ for an evaporating disk. Also shown is a fit to Eq. (A2) with $(d_0D)$ as a fitting parameter.

It is apparent that both estimates of $R_2^*$ are consistent with our simulation results.

## IV. SUMMARY

For the case of circular growth geometry, quantitative agreement was found between the simulation results and those of a linear stability analysis. In the case of the flat growth geometry, a linear regime was observable only by using long-range interactions. We demonstrated that a long-range force suppresses the instability thus making the linear regime longer in time. The measured dispersion relation shows qualitative agreement with linear stability analysis, but only in a regime $kd_0 \leq 1$ where the modes are damped by the surface tension rather than by the diffusion of latent heat. With this proviso, and taken together with the steady-state results reported earlier [15], the agreement with linear stability analysis give further support to our model as capturing the essential physics of the phase boundary. Our lattice-gas model thus provides an alternative method for tackling the difficult problem of pattern formation during solidification.

## ACKNOWLEDGMENTS

This work was supported by the Natural Sciences and Engineering Research Council of Canada, and les Fonds pour la Formation de Chercheurs et l'Aide á la Recherche de la Province du Québec.

## APPENDIX

If the initial radius of the droplet $R = R_0$ is larger than the critical nucleation radius $R_c$, it will start to grow. In two dimensions, $R_c$ is usually expressed as $R_c = \gamma/\triangle E_b$ where $\gamma$ is the surface free energy and $\triangle E_b$ is the bulk free energy difference. Values for $\gamma(T)$ and $\triangle E_b(T)$ are available, respectively, from perturbative analysis of the regular nearest-neighbor 2D Ising model [33] and from mean-field analysis.

When $R > R_c$, the growing droplet will remain circularly stable until $R \sim R_m^*$ where $m$ denotes the dominant mode of the instability. It will then become unstable and begin to grow finger formations typical of the Mullins-Sekerka instability (see Fig. 5). Expressions for $R_m^*$ can be obtained from linear stability analysis of the circular interface.

Assuming a perfect circle of radius $R_0(t)$, Eqs. (1)–(3) have unperturbed solutions for $u(r)$

$$u_0(r) = \begin{cases} (\Lambda R_0 - d_0)/r - \Lambda, & r \geq R_0 \quad \text{(liquid)} \\ -d_0/R_0, & r \leq R_0 \quad \text{(solid)}. \end{cases} \tag{A1}$$

Using the continuity equation, we find the unperturbed interface velocity to be

$$v_{R_0} \equiv \frac{dR_0}{dt} = -D\nabla u \cdot \hat{\mathbf{r}} = \frac{D(\Lambda R_0 - d_0)}{R_0^2}, \tag{A2}$$

where $\hat{\mathbf{r}}$ is the radial interface normal vector. From the limit $v_{R_0} = 0$, an equivalent expression for the critical

nucleation radius is then obtained. It becomes $R_c = d_0/\Lambda$, where $d_0$ is the capillary length and $\Lambda = -u(\infty)$ is the dimensionless undercooling at infinity.

Equation (A2) describes the rate of growth of a stable disk. A small perturbation is then introduced at the disk interface

$$R(\theta) = R_0 + \sum_m \rho_m \cos(m\theta) e^{\omega_m t}; \tag{A3}$$

with the perturbed thermal field having a similar form

$$u(r) = u_0(r) + \sum_m u_m(r) \cos(m\theta) e^{\omega_m t} \tag{A4}$$

and where

$$u_m(r) = \begin{cases} A_m r^{-m}, & r > R_0 \quad \text{(liquid)} \\ B_m r^m, & r \le R_0 \quad \text{(solid)}. \end{cases}$$

Linearizing the expression for the perturbed interface, we evaluate the growth rates of the modes to be

$$\omega_m \simeq \frac{v_{R_0}(m-1)}{R_0} \left[ 1 - \frac{2Dd_0}{v_R R_0^2} m(m-1) \right], \tag{A5}$$

where growth occurs for $m \ge 2$. The instability radius for a given mode $m$ is then defined by the limit $\omega_m \to 0$;

$$(R_m^*)^2 = m(m+1)\frac{2Dd_0}{v_R} \qquad (m \ge 2). \tag{A6}$$

Substituting Eq. (A2) into Eq. (A6) and using $R_c = d_0/\Lambda$, this can be rewritten as

$$\frac{R_m^*}{R^*} = 2m(m+1) + 1 \qquad (m \ge 2). \tag{A7}$$


[1] P. Saffman and G. Taylor, Proc. R. Soc. London Ser. A **245**, 312 (1958).
[2] D. Bensimon, L. Kadanoff, S. Liang, B. Shraiman, and C. Tang, Rev. Mod. Phys. **58**, 977 (1986).
[3] G. Homsey, Ann. Rev. Fluid Mech. **19**, 271 (1987).
[4] H. Biloni, *Physical Metallurgy*, 3rd ed. (North-Holland, Amsterdam, 1983),Vol. 1.
[5] W. Kurz and F. Fisher, *Fundamentals of Solidification*, (Trans Tech Publications, Aedermannsdorf, Switzerland, 1984).
[6] S. Huang and M. Glicksman, Acta Metall. **29**, 717 (1981).
[7] W. Mullins and R. Sekerka, J. Appl. Phys. **34**, 323 (1963).
[8] W. Mullins and R. Sekerka, J. Appl. Phys. **35**, 444 (1964).
[9] J. Langer, in *Lectures in the Theory of Pattern Formation, Chance and Matter*, Proceedings of the Les Houches Summer School Session 46, Amsterdam, edited by J. V. J. Souletie and R. Stora (North-Holland, Amsterdam, 1986).
[10] D. Kessler, J. Koplik, and H. Levine, Adv. Phys. **37**, 255 (1988).
[11] Y. Saito, G. Goldbeck-Wood, and H. Müller-Krumbhaar, Phys. Rev. A **38**, 2148 (1988).
[12] H. Guo and D. Jasnow, Phys. Rev. A **34**, 5027 (1986).
[13] D. Jasnow and J. Viñals, Phys. Rev. A **40**, 3864 (1989).
[14] D. Jasnow and J. Viñals (unpublished).
[15] R. Harris and M. Grant, J. Phys. A **23**, L567 (1990).
[16] L. Kadanoff, J. Stat. Phys. **39**, 267 (1985).
[17] S. Liang, Phys. Rev. A **33**, 2663 (1986).
[18] C. Tang, Phys. Rev. A **31**, 1977 (1985).
[19] H. Guo and D. Hong, Phys. Rev. A **41**, 2995 (1990).
[20] R. Harris and M. Grant, Phys. Rev. B **38**, 9323 (1988).
[21] L. Jörgenson, R. Harris, and M. Grant, Phys. Rev. Lett. **63**, 1693 (1989).
[22] R. Harris, L. Jörgenson, and M. Grant, Phys. Rev. A **45**, 1024 (1992).
[23] L. Jörgenson, R. Harris, M. Grant, and H. Guo, Phys. Rev. E **47**, 1235 (1993).
[24] L. Jörgenson and R. Harris, Phys. Rev. E **47**, 3504 (1993).
[25] J. Langer, Rev. Mod. Phys. **52**, 1 (1980).
[26] K. Binder, J. Chem. Phys. **79**, 6387 (1983).
[27] K. Binder, Phys. Rev. A **29**, 341 (1984).
[28] R. Harris, Phys Lett. **111A**, 299 (1985).
[29] N. Metropolis, A. Rosenbluth, M. Rosenbluth, A. Teller, and E. Teller, J. Chem. Phys. **21**, 1087 (1953).
[30] M. Creutz, Phys. Rev. Lett. **50**, 1411 (1984).
[31] P. Hohenberg and B. Halperin, Rev. Mod. Phys. **49**, 435 (1977).
[32] M. Grant, Phys. Rev. B **37**, 5705 (1988).
[33] C. Rottman and M. Wortis, Phys. Rev. B **24**, 6274 (1981).